



Contents lists available at ScienceDirect

Comptes Rendus Chimie

www.sciencedirect.com



Full paper/Mémoire

## New *p*-aminophenol-based dendritic melamines. Iterative synthesis, structure, and electrochemical characterisation

Cristina Morar <sup>a</sup>, Graziella Liana Turdean <sup>b</sup>, Attila Bende <sup>c</sup>, Pedro Lameiras <sup>d</sup>,  
Cyril Antheaume <sup>e</sup>, Liana Maria Muresan <sup>b, \*\*</sup>, Mircea Darabantu <sup>a, \*</sup>

<sup>a</sup> Babes-Bolyai University, Department of Chemistry, 11 Arany János St., 400028 Cluj-Napoca, Romania

<sup>b</sup> Babes-Bolyai University, Department of Chemical Engineering, 11 Arany János St., 400028 Cluj-Napoca, Romania

<sup>c</sup> National Institute for Research and Development of Isotopic and Molecular Technologies, Molecular and Biomolecular Physics Department, 65-103, Donath St., PO Box 700, 400293 Cluj-Napoca 5, Romania

<sup>d</sup> University of Reims Champagne-Ardenne, ICMR, UMR 7312, BP 1039, 51687 Reims, France

<sup>e</sup> University of Strasbourg, Faculty of Pharmacy, 74, route du Rhin, BP 60024, 67401 Illkirch cedex, France

### ARTICLE INFO

#### Article history:

Received 2 May 2016

Accepted 11 July 2016

Available online xxxx

#### Keywords:

*p*-Aminophenol

Cyclic voltammetry

Dendrimers

DFT

Melamine

### ABSTRACT

Avoiding any protective–deprotective step, the synthesis of new (G-0, -1, -2) dendritic melamines is reported. Their construction consisted of chemoselective S<sub>N</sub>2–Ar amination of cyanuric chloride with *p*-aminophenol (peripheral unit) and piperazine or 4,4'-bipyridine (linkers). This novel class of amino-*s*-triazines is primarily investigated by DFT calculations (optimal geometry and electronic structure) in tandem with (VT) <sup>1</sup>H NMR spectroscopy providing details of the rotational diastereomerism about the C(*s*-triazine)-N(exocyclic) partial double bonds, solvation effects and conformation of the linkers. These data are subsequently exploited in electrochemical investigations (cyclic voltammetry on the Pt electrode/DMSO, 0.1 M KCl). Two reversible electron-transfer phenomena have been observed. Thus, depending on the variable  $\pi$ -deficiency strength of the *s*-triazine ring acting as the EWG on the adjacent NH group and the ability of the latter to undergo redox processes in tandem with the phenolic *p*-HO group, two electrochemical pathways are proposed, namely the *p*-benzoquinonimine route and the electropolymerization route.

© 2016 Académie des sciences. Published by Elsevier Masson SAS. All rights reserved.

### 1. Introduction

There are multidisciplinary approaches nowadays focused on *N*-substituted amino-*s*-triazines with hydroxy-phenyl units [1–4]. Actually, the use of *p*-aminophenol in the classic S<sub>N</sub>2–Ar amination of cyanuric chloride, yielding *m*-trivalent branched melamine (2,4,6-triamino-1,3,5-triazine)-polycarbonates, has been known since 1987 [1a].

Later on, the patented applications of these macromolecules as new plasticizers promoted subsequent findings in the domain of organic materials, for example thermoplastic compounds [1b] and ingredients for lubricants or lubricant compositions [1c,1d]. More recently, the synthesis and structural properties of arborescent architectures built around trimesic(1,3,5-tricarbonylbenzene) [2a] or *s*-triazine [2b] cores by means of *p*-aminophenol units were also described. The first synthesis of a (G-1) dendritic melamine comprising *p*-aminophenol as an internal linker and 2-aminopyridine as a peripheral unit, reported by Gamez and co-workers in 2002, targeted a novel polydentate and polynucleating *N*-donor ligand [3]. On the other hand, it is also worth mentioning the bioimpact of some *N*-substituted

\* Corresponding author.

\*\* Corresponding author.

E-mail addresses: limur@chem.ubbcluj.ro (L.M. Muresan), darab@chem.ubbcluj.ro (M. Darabantu).

melamines with (*O*-protected)hydroxyphenyl motifs conjugating 4-aminoquinoline as antimalarial agents [4].

In the above multi-facet context, we consider of interest to extend our expertise in the field of dendritic melamines' preparation and structure [5] (including electrochemical approach [5e]) by using a versatile-redox and bidentate nucleophile, *p*-aminophenol. The last one was designed to play the role of a peripheral unit, in an iterative-convergent type synthesis, a strategy previously developed by Simanek's group [6]. Next, cyclic voltammetry has been employed to study the electrochemical behaviour of the first (G-2) dendrimer encompassing *p*-aminophenol as the peripheral unit and of its precursors on the Pt electrode in DMSO.

To our knowledge, no similar investigation has been reported so far.

Indeed, dendrimers containing redox active functionalities are especially important because of their interesting electron-transfer properties [7]. Thus, the peripheral redox active units, undergoing multiple electron transfer and redox properties, can be modulated by the size and nature of the dendritic branches [8]. Aminophenols are well-documented electrochemically active compounds since they have two groups ( $-\text{NH}_2$  and  $-\text{OH}$ ), which could be oxidized [9]. Moreover, the electropolymerization of *p*-aminophenol itself on a Pt electrode in organic solvents, providing a soluble electroactive polymer, was also reported [9a].

## 2. Results and discussion

### 2.1. Synthesis

The chemistry we followed is resumed in Scheme 1 and the reaction conditions are presented in Table 1.

First, we tested the chemoselectivity in the amination of cyanuric chloride by *p*-aminophenol (*p*-AP) in the synthesis of melamine **1a** (Table 1, entry 1) versus that of chlorodiamino-*s*-triazine **1b** (Table 1, entries 2 and 3). Although the preparation of **1a** was of applied interest for several authors [1a–d,3], in our hands only the procedure of Negoro and Kawata [1c,1d] gave satisfaction as excellent and reproducible yield, 91% [10]. Under similar but milder conditions (Table 1, entry 2), amination of cyanuric chloride performed with two molar equiv. of *p*-aminophenol yielded compound **1b** contaminated with traces of melamine **1a**. Hence, **1b** required purification by column chromatography when an important loss of the material due to its relative retention on silica gel was observed, affecting the yield. Our option of choice was then the method of Bhat and co-workers [4b,4c] (Table 1, entry 3) which produced **1b** with good yield, 73%, in an expeditious manner.<sup>1</sup> Compound **1b** exhibited moderate solubility in organic solvents usually recommended for the

synthesis of amino-*s*-triazines (THF, 1,4-dioxane, acetone etc.) [6], most likely because of its high polarity. That is, in order to adopt a protective–deprotective strategy, **1b** was diacetylated (Table 1, entry 4) in high yield (90%) with complete *O,O'*-chemoselectivity. Unfortunately, the resulting *O,O'*-diacetyl derivative **2** was inappropriate for our envisaged iterative syntheses (Scheme 1). Thus, the reaction between **2** and piperazine (not depicted in Scheme 1), besides the expected amination of the *s*-triazine chlorine, consisted as well of the partial transfer of the acetyl group (*O*-phenol  $\rightarrow$  *N*-piperazine) affording a multicomponent reaction mixture. By contrast, compound **2** was of crucial relevance in electrochemical investigations (Section 3.1.) To conclude, for the present report, we had to manage our strategy limited to (G-0) chlorodendrion **1b**.

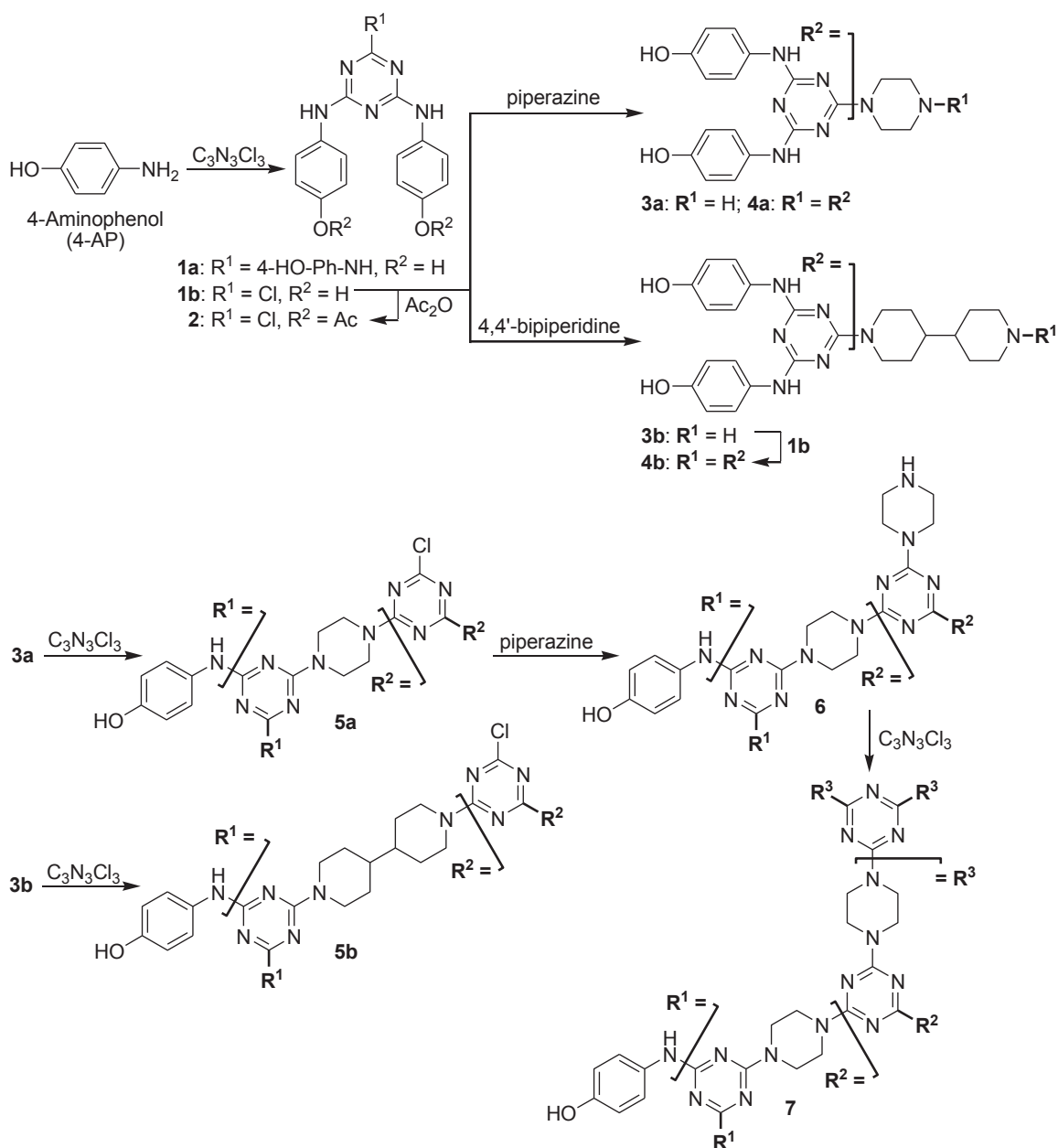
Based on our earlier published methodology [5a–d], the chemoselective mono-attachment of piperazine, as the first linker, to **1b** (Table 1, entry 5) gave the (G-0) melamine **3a**. Thus, during the portionwise addition of **1b** to a 300% molar excess of piperazine, the TLC monitoring of the amination revealed a very clean evolution towards **3a** only, i.e. the complete absence of the dimeric melamine **4a** as a side product (Scheme 1). As shown in Table 1 (entry 5), it was the single situation, that of **3a**, in which both techniques for its purification (direct crystallisation or column chromatography on partially deactivated silica gel) provided good and comparable quantitative results. Our attempt to prepare compound **3a** by applying the method of Bath and co-workers [4c] (equimolar ratio **1b**: piperazine, 82% claimed yield of **3a**) failed (Table 1, entry 6). The resulting mixture **3a** (minor) and **4a** (major) could be successfully separated by column chromatography.

The protocol for the non-symmetric anchorage of the 4,4'-bipiperidine linker to **1b** (Table 1, entry 7) producing melamine **3b** was the same as in the case of piperazine against **1b** but the amination reached completion in a much longer time. The yield of **3b** was critically influenced by the work-up used for its isolation as a pure analytical sample, 86% (direct crystallisation from boiling ethanol) versus 45% (column chromatography on a partially deactivated silica gel). Our tentative explanation relates, once again, to the high relative retention on column chromatography of **3b** (see also the next examples).

The symmetric analogue **4b** of **3b** was also prepared from the latter in reaction with **1b** (Table 1, entry 8).

As expected, the one-pot synthesis of (G-1) chlorodendrons **5a** and **5b** (Table 1, entries 9 and 10 respectively) required mild conditions for the first step amination. However, the second step was mandatory to taxing reaction parameters (36 h in refluxing 1,4-dioxane), suggesting the low reactivity of the intermediates due to their strong solvation in the depicted solvents. Except for DMF and DMSO, both compounds **5a** and **5b** manifested low solubility in common organic volatile solvents. Therefore, in order to avoid the loss of the material on column chromatography (i.e. compound **5b**, 47% yield), purifications were successfully realised by crystallisations from boiling ethanol (86% optimised yield of **5b**). Even so, the (G-1) chlorodendrion **5b** showed an unexpected weak reactivity in subsequent aminations attempted

<sup>1</sup> Our analytical sample **1b** was different with respect to that of Bath and co-workers [4b,4c]. Our diagnosis concerned the aspect (white powder in our case against reported black crystals), melting point (343.7–344.1 °C in our case, against reported 251–252 °C) and the appropriate solubility for NMR analysis (only DMSO-*d*<sub>6</sub> in our case, against reported CDCl<sub>3</sub>); see Figs. SI-4–7 in SI (Supporting information). Similar observations apply for compound **3a** with respect to the sample of Bath and co-workers [4c]; see Figs. SI-12–14.



Scheme 1.

with piperazine or 4,4'-bipiperidine. Therefore, for the present work, we had to limit the study by using henceforth (G-1) chlorodendron **5a** only.

In so doing, we effected, in accordance with the same methodology as that in the case of (G-0) melamine **3a**, the selective anchorage of the next piperazine linker on **5a** (Table 1, entry 11) and obtained (G-1) melamine **6**. We detected no dimeric melamine as a side product and isolated **6** by column chromatography on a partially deactivated silica gel or, as an optimal decision, by crystallisation (88% yield).

The final installation of the trivalent *s*-triazine core on **6** (Table 1, entry 12) was performed in a one-pot procedure

with good global yield (85%). Compound **7**, the first (G-2) dendrimer comprising *p*-aminophenol as the peripheral unit, could not be eluted on TLC due to its low solubility in common organic solvents. Its identity was fully confirmed by spectral methods.

## 2.2. Preliminary structural assignments

As early as 1971 [11a], it was established that the C(*s*-triazine)-N(exocyclic) linkages in amino-*s*-triazines have a partial double bond character due to the  $p(N) \rightarrow \pi(C=N)$  conjugation between the lone pair of the exocyclic *N*-atom in conjunction with the high  $\pi$ -deficient *s*-triazine ring

**Table 1**Reaction conditions and results in the synthesis of compounds **1–7** (see Scheme 1).

Entry	Reaction	Conditions	Products, yields (%) and isolation: direct crystallisation (d.c.), column chromatography on silica gel (c.c.) <sup>a</sup>
1	<i>p</i> -AP → <b>1a</b>	i) 0.30 equiv C <sub>3</sub> N <sub>3</sub> Cl <sub>3</sub> , butanone/0–5 °C (30 min); ii) 1.00 equiv AcONa, H <sub>2</sub> O/5–9 °C (30 min); iii) reflux (3 h)	<b>1a</b> : 91 (d.c.)
2	<i>p</i> -AP → <b>1b</b>	i) 0.50 equiv C <sub>3</sub> N <sub>3</sub> Cl <sub>3</sub> , butanone/0–5 °C (30 min); ii) 1.00 equiv AcONa, H <sub>2</sub> O/5–9 °C (30 min); iii) r.t. (24 h)	<b>1b</b> : 56 (c.c.)
3	<i>p</i> -AP → <b>1b</b>	i) 0.50 equiv C <sub>3</sub> N <sub>3</sub> Cl <sub>3</sub> , acetone/0–5 °C (2 h); ii) 1.00 equiv NaHCO <sub>3</sub> , H <sub>2</sub> O/5–9 °C; iii) 45 °C (3 h); r.t. (15 h)	<b>1b</b> : 73 (d.c.) <sup>b</sup>
4	<b>1b</b> → <b>2</b>	2.23 equiv Ac <sub>2</sub> O, 1.00 equiv K <sub>2</sub> CO <sub>3</sub> , THF/r.t. (4 h); reflux (10 h)	<b>2</b> : 90 (d.c.)
5	<b>1b</b> → <b>3a</b>	4.00 equiv piperazine, 1.00 equiv K <sub>2</sub> CO <sub>3</sub> , THF/r.t. (15–20 h)	<b>3a</b> : 83 (c.c.); 85 (d.c.)
6	<b>1b</b> → <b>3a</b> , <b>4a</b>	1.00 equiv piperazine, 1.00 equiv K <sub>2</sub> CO <sub>3</sub> , 1,4-dioxane/reflux (8 h)	<b>3a</b> : 17 (c.c.); <b>4a</b> 83 (c.c.) <sup>c</sup>
7	<b>1b</b> → <b>3b</b>	4.00 equiv 4,4'-bipiperidine, 1.00 equiv K <sub>2</sub> CO <sub>3</sub> , THF/r.t. (36–42 h)	<b>3b</b> : 45 (c.c.); 86 (d.c.)
8	<b>3b</b> → <b>4b</b>	1.00 equiv <b>1b</b> , 1.00 equiv K <sub>2</sub> CO <sub>3</sub> , 1,4-dioxane/reflux (13 h)	<b>4b</b> : 64 (d.c.)
9	<b>3a</b> → <b>5a</b>	i) 1.00 equiv <b>3a</b> , 1.00 equiv K <sub>2</sub> CO <sub>3</sub> , THF/–15 °C (20–24 h); ii) 1.00 equiv <b>3a</b> , 1.00 equiv K <sub>2</sub> CO <sub>3</sub> , THF/r.t. (20–24 h); iii) 1,4-dioxane, reflux (36 h)	<b>5a</b> : 90 (d.c.)
10	<b>3b</b> → <b>5b</b>	i) 1.00 equiv <b>3b</b> , 1.00 equiv K <sub>2</sub> CO <sub>3</sub> , THF/–15 °C (22 h); ii) 1.00 equiv <b>3b</b> , 1.00 equiv K <sub>2</sub> CO <sub>3</sub> , THF/r.t. (24 h); iii) 1,4-dioxane, reflux (36 h)	<b>5b</b> : 47 (c.c.); 86 (d.c.)
11	<b>5a</b> → <b>6</b>	i) 4.00 equiv piperazine, 1.00 equiv K <sub>2</sub> CO <sub>3</sub> , THF/r.t. (20–30 h); ii) reflux (12 h)	<b>6</b> : 55 (c.c.); 88 (d.c.)
12	<b>6</b> → <b>7</b>	i) 0.30 equiv C <sub>3</sub> N <sub>3</sub> Cl <sub>3</sub> , 1.00 equiv K <sub>2</sub> CO <sub>3</sub> , 1,4-dioxane/r.t. (24 h); ii) reflux (48 h)	<b>7</b> : 85 (d.c.)

<sup>a</sup> On partially deactivated silica gel (eluent EtOH: aq. NH<sub>3</sub> 25%) for compounds **3a**, **4a**, **3b** and **6**.<sup>b</sup> 67% Yield according to Refs. [4b] and [4c].<sup>c</sup> Partial conversions of **1b** into the depicted compounds, calculated based on effective amounts isolated by column chromatography. Full details of these syntheses are given in the SI (Supporting information).

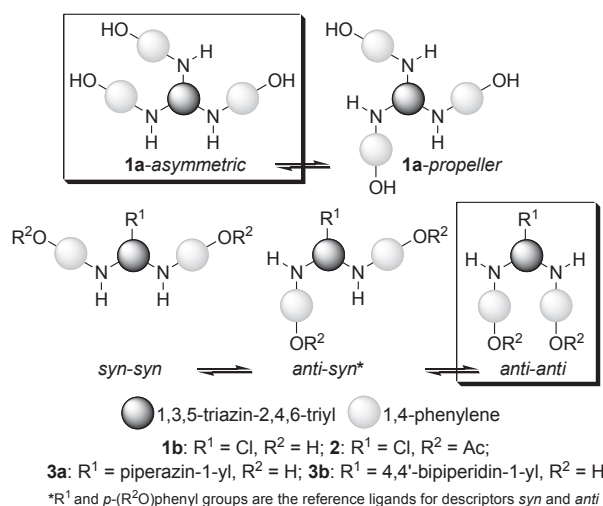
[11]. There is a restricted rotation thus induced. Variable temperature NMR spectroscopy is an appropriate technique for monitoring this stereodynamism [12], including examples of arylamino-*s*-triazines [12d–f,12h]. As for other amino-*s*-triazines, in the case of monomeric (G-0) dendrons **1a**, **1b**, **2**, **3a** and **3b**, at room temperature, a topological idealised model [5a–d,12g] predicted, for **1a**, a two term rotational diastereomerism (*asymmetric* ⇌ *propeller*) and three terms (*syn*–*syn* ⇌ *anti*–*syn* ⇌ *anti*–*anti*) for **1b**, **2**, **3a** and **3b** (Scheme 2).

Therefore, before any electrochemical investigation, a study by means of DFT [13–20] calculations in solution (DMSO) was implemented for compounds **1a**, **1b**, **2**, **3a**, **3b** and **7**, selected as the representative. The results are shown in Tables 2 and 3 and Fig. 1 together with those referring to the starting *p*-aminophenol (*p*-AP) and its *N*-acetyl derivative, the well-known anti-inflammatory drug *paracetamol* (PA).

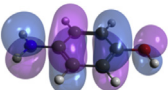
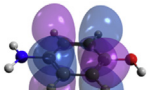
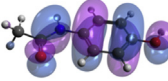
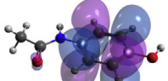
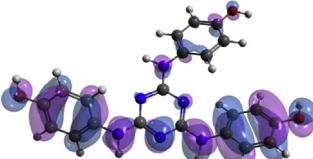
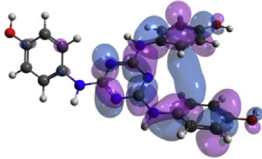
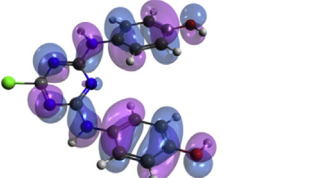
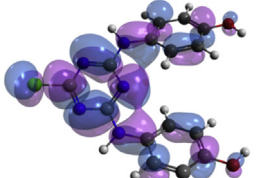
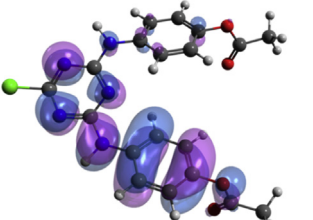
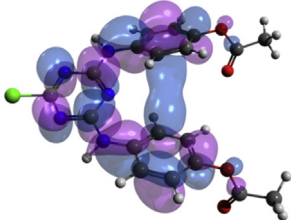
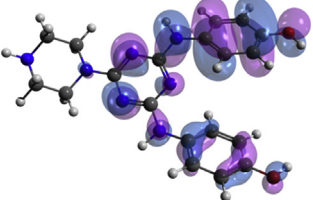
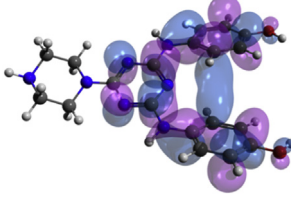
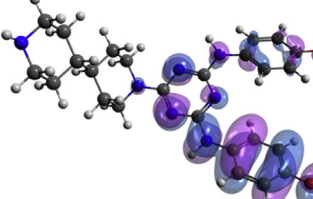
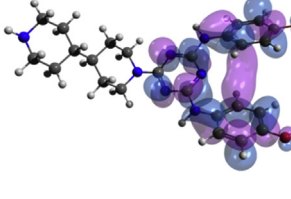
They deserved the below comments:

- (i) The optimised geometry of melamine **1a** was found to be of type *asymmetric* (Table SI-1, Supporting information); meanwhile *anti*–*anti* was the preferred rotameric arrangement adopted by the *p*-(R<sup>2</sup>O)phenyl units in compounds **1b**, **2**, **3a** and **3b** in DMSO (Table SI-2, Table 2). The same *anti*–*anti* stereochemistry was *local* at the periphery of dendrimer **7** which disclosed a vaulted *global* shape [21] (Fig. 1).

- (ii) The increasing order of ε<sub>HOMO</sub> energies (Table 2) correlated with the decreasing strength of the EWG *N*(O)-substituting the *p*-(R<sup>2</sup>O)phenylamino units (Scheme 1), namely acetyl and variable π-deficient *s*-triazine ring, i.e. **2** < *paracetamol* ~ **1b**. However, an

**Scheme 2.**

**Table 2**Full geometry optimisation and calculated  $\epsilon_{\text{HOMO}}$ ,  $\epsilon_{\text{LUMO}}$  in *p*-aminophenol (*p*-AP), *paracetamol* (PA) and of (G-0) dendrons **1a**, **1b**, **2**, **3a** and **3b** in DMSO.<sup>a</sup>

No.	HOMO	LUMO	$\epsilon_{\text{HOMO}}$ (eV)	$\epsilon_{\text{LUMO}}$ (eV)	Gap (eV)
<i>p</i> -AP			-6.24	+0.68	6.92
PA			-7.00	+0.50	7.50
<b>1a</b>			-6.81	+0.31	7.12
<b>1b</b>			-6.99	-0.03	6.96
<b>2</b>			-7.47	-0.23	7.24
<b>3a</b>			-6.80	+0.35	7.15
<b>3b</b>			-6.81	+0.35	7.16

<sup>a</sup> The full geometry optimisation has been carried out at the DFT level of theory considering the M06-2X [13] exchange-correlation functional together with the def2-TZVP [14] basis set in the presence of a solvent environment implemented in the Gaussian 09 [15] program package. The solvent effects have been taken into account via the Polarizable Continuum Model (PCM) using the integral equation formalism variant (IEFPCM) [16] considering the DMSO ( $\epsilon = 46.826$ ) as the solvent environment.

equalisation of  $\epsilon_{\text{HOMO}}$  energies in the melamine series **1a** ~ **3a** ~ **3b** resulted from calculation. Obviously, the highest  $\epsilon_{\text{HOMO}}$  level was that of *p*-aminophenol.

(iii) The partial double bond nature of connexions C(s-triazine)-N(exocyclic) was disclosed by Bond Order (BO)

values ranging between 1.20 and 1.25, anyhow much greater than those of connexions C(Ph)-NH. The calculated Bond Lengths (BLs) fully supported their inverted dependence with respect to the corresponding BO indexes (Table 3).



**Table 3**

Indicative Bond Order (BO) indexes, Bond Lengths (BLs) and Lone Pair (LP) orbital populations in *p*-aminophenol (*p*-AP), *paracetamol* (PA) and (G-O) dendrons **1a**, **1b**, **2**, **3a** and **3b** in DMSO.

No.	C(s-triazine)-N(H)		C(Ph)-N(H)		C(s-triazine)-N<		Lone Pair (LP) orbital populations (e) <sup>a</sup>			
	BO <sup>b</sup>	BL (Å) <sup>c</sup>	BO	BL (Å)	BO	BL (Å)	N(H)	O(H, Ac)	-N<	s-Triazine N(1, 3, 5)
<i>p</i> -AP	—	—	1.15	1.375	—	—	1.82	3.88	—	—
PA	—	—	1.05	1.410	—	—	1.64	3.86	—	—
<b>1a</b>	1.21	1.353	1.04	1.411	—	—	1.68	3.86	—	1.90
<b>1b</b>	1.25	1.351	1.03	1.410	—	—	1.64	3.86	—	1.90
<b>2</b>	1.24	1.343	1.04	1.406	—	—	1.64	3.76	—	1.90
<b>3a</b>	1.20	1.360	1.04	1.407	1.23	1.353	1.68	3.86	1.67	1.90–1.91
<b>3b</b>	1.20	1.361	1.04	1.407	1.23	1.352	1.68	3.86	1.67	1.90–1.91

<sup>a</sup> Obtained by considering the NBO electron population analysis at the M06-2X/def2-TZVP level of theory where *e* is the elementary electric charge carried by a single electron.

<sup>b</sup> Calculated at the M06-2X/def2-TZVP level of theory considering the Wiberg definitions of bond order (see Ref. [19]) implemented in the NBO analysis module.

<sup>c</sup> Calculated at the M06-2X/def2-TZVP level of theory.

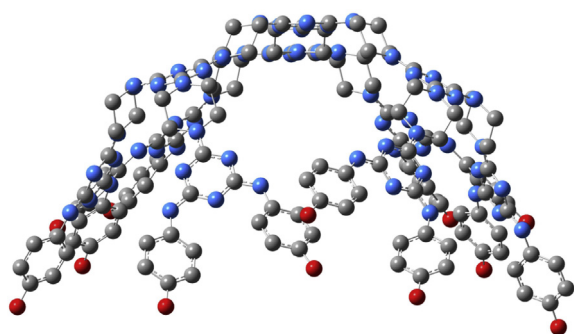


**Fig. 1.** The optimised geometry structure of compound **7** obtained at M06-2X/def2-TZVP level of theory [14] (the H atoms were omitted for reasons of simplicity).

(iv) The lowest nitrogen Lone Pair (LP) orbital populations (1.64–1.68) were found in LPN(H) →  $\pi$ (C=O) (*paracetamol*) and LPN(exocyclic) →  $\pi$ (s-triazine) conjugated compounds **1a**, **1b**, **2**, **3a** and **3b**. The LP orbital

population of the phenolic oxygen was less diminished (3.76–3.88) as a consequence of the LPO(H, Ac) →  $\pi$ (Ph) or LPO →  $\pi$ (C=O) delocalisation.

Furthermore, data issued from (VT) <sup>1</sup>H NMR investigations (Table 4) completed those provided by theoretical anticipations.

Unsurprisingly, the most  $\pi$ -deficient diamino-chloro-s-triazines **1b** and **2** displayed, at room temperature, the most convincing <sup>1</sup>H NMR spectral appearance, consistent with the nearly frozen nature of their rotational equilibria (Scheme 2) on the NMR time scale (Figs. SI-4 and SI-8). In contrast, under the same conditions, the rotamerism of all melamines (G-O, -1, -2) was identified by NMR as a classically entitled “slow exchange status between (un)equally populated sites” [22]. Upon heating to 80–90 °C (Table 4), all compounds became single mediated structures, in a fast freely rotating status about all C(s-triazine)-N(exocyclic) bonds.

Temperature Gradients (TGs) of the NH protons were also indicative because they revealed the influence of different types of *N*-ligands on solvation. Although this

**Table 4**

Relevant (VT) <sup>1</sup>H and 2D-<sup>1</sup>H-DOSY-NMR data (500 MHz, DMSO-*d*<sub>6</sub>) of compounds **1a**, **1b**, **2**, **3–5a**, **3–5b**, **6** and **7**.

No.	Relevant $\delta_H$ values (ppm) (298 K)		Relevant $\delta_H$ values (ppm) (363 K)		Temperature gradients (TGs) as $(\Delta\delta_{NH}/\Delta T) \times 10^3$ (ppb/K) <sup>a</sup>	<i>D</i> (μm <sup>2</sup> /s)	<i>d</i> <sub>H</sub> <sup>b</sup> (nm)
	NH	OH	NH	OH			
<b>1a</b>	8.74	9.06	8.37	8.74	–5.69	152	1.44
<b>1b</b>	9.70	9.27	9.46	8.91	–3.69	218	1.00
	9.83	—	—	—	–5.69	—	—
	9.91 <sup>c</sup>	—	—	—	–6.92	—	—
<b>2</b>	10.18	—	9.97 <sup>d</sup>	—	–3.82	230	0.95
	10.34 <sup>c</sup>	—	—	—	–6.73	—	—
<b>3a</b>	8.71	9.01	8.34	8.68	–5.69	152	1.44
<b>4a</b>	8.81	9.04	8.41	8.69	–6.15	137	1.59
<b>3b</b>	8.72	9.02	8.33	8.66	–6.00	131	1.67
<b>4b</b>	8.72	9.01	8.36 <sup>d</sup>	8.70	–6.55	125	1.75
<b>5a</b>	8.83	9.04	8.54	8.79	–4.46	90	2.43
<b>5b</b>	8.72	9.01	8.32 <sup>d</sup>	8.66	–7.27	72	3.03
<b>6</b>	8.78	9.04	8.47	8.78	–4.77	82	2.66
<b>7</b>	8.79	9.05	8.39	8.70	–6.15	70	3.12

<sup>a</sup> Calculated as  $[(\delta_H^{298K} - \delta_H^{363K}) / (298 K - 363 K)] \times 10^3 < 0$ .

<sup>b</sup> *d*<sub>H</sub> (Hydrodynamic diameter) issued from *D* [diffusion coefficient observed in 2D-<sup>1</sup>H-DOSY NMR charts in 5 mM DMSO-*d*<sub>6</sub> ( $\eta$ , dynamic viscosity  $2.00 \times 10^{-3}$  kg m<sup>–1</sup> s<sup>–1</sup>) at 298 K] by applying the Stokes–Einstein equation.

<sup>c</sup> Multiple  $\delta_H$  values due to more than one (*anti*–*anti*) species found in a frozen rotational equilibrium in agreement with the highest  $\pi$ -deficiency of the *s*-triazine ring in the analysed series (Scheme 2, Figs. SI-4 and SI-8).

<sup>d</sup> At 353 K.

parameter is appropriate for amide  $-N(H)-C(=O)- \leftrightarrow -N^+(H)=C(-O^-)-$  protons in peptides and proteins [23], it can also be applied to amino-*s*-triazines,  $-N(H)-C(=N)- \leftrightarrow -N^+(H)=C(-N^-)-$  as established by Simanek and Moreno [21b]. Following this extrapolation, if TG values of “amide-like” protons in amino-*s*-triazines are more negative than  $-4$  ppb/K in strong hydrogen bond acceptor solvents, such as DMSO- $d_6$  [12g], the NH groups are exposed to the solvent rather than forming intramolecular hydrogen bonds. On the other hand, a TG value less negative than  $-4$  ppb/K indicates that the NH group preferentially forms intramolecular hydrogen bonds at room temperature. If so, besides the normal aptitude for binding of *p*-HO phenolic functionalities, the contribution to solvation of NH groups, i.e.  $Me_2S=O \cdots H \cdots N<$ , was also significant. Indeed, as one can see, almost all TGs in Table 4 were more negative than  $-4$  ppb/K in conjunction with an *anti-anti* arrangement of phenolic (peripheral) units (Scheme 2, Table 2) in all types of compounds. Consistent with some of our previous data [5b], when the rotamerism was  $^1H$  NMR detected as a mixture of stereoisomers (compounds **1b** and **2**, Table 4), this situation disclosed the major rotamer *anti-anti* (Table 2) being the most solvated as well (TGs as  $-6.92$  ppb/K and  $-6.73$  ppb/K, respectively, Figs. SI-4 and SI-8).

Surprisingly, the different conformational nature of the internal linker, anancomeric<sup>2</sup> [22b] (rigid, 4,4'-bipiperidin-1,1'-diyl) against chair  $\rightleftharpoons$  chair flipping (piperazine-1,4-diyl) determined lower TGs in **4b** ( $-6.55$  ppb/K) and **5b** ( $-7.27$  ppb/K) with respect to **4a** ( $-6.15$  ppb/K) and **5a** ( $-4.46$  ppb/K) (Scheme 3).

Dimeric (G-O) melamines **4a** and **4b** were more  $Me_2S=O \cdots H \cdots N<$  solvated in comparison with their monomeric precursors **3a** (TG as  $-5.69$  ppb/K) and **3b** (TG as  $-6.00$  ppb/K), respectively.

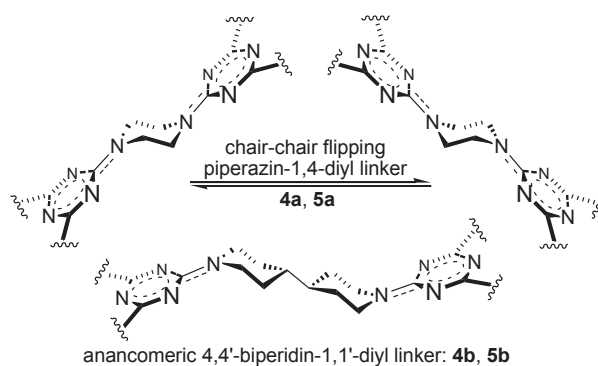
To what extent the above structural findings have a corresponding electrochemical impact, we will discuss hereafter.

## 2.3. Electrochemical characterisation

### 2.3.1. Cyclic voltammetry

Next, the electrochemical behaviour of our *p*-aminophenol-based amino-*s*-triazines was investigated by means of cyclic voltammetry. The cyclic voltammograms recorded on the Pt electrode in DMSO, 0.1 M KCl solution are presented in Fig. 2.

Except for compounds **2** and **7**, all voltammograms revealed the presence of a single well-defined anodic oxidation peak A1 closely located around 0 V versus Ag/AgCl,  $KCl_{sat}$ . By contrast, 1–3 cathodic reduction peaks, C1–3, were disclosed as C1 and C3 (*paracetamol* and compounds **1b**, **3b**, and **6**), C2 and C3 (compound **1a**) or C1, C2 and C3 (compounds **3a**, **4a**, **4b**, **5a** and **5b**). The variable incidence of the reduction peaks C1 and/or C2 was attributed to the successive reduction of the species



Scheme 3.

produced during electrochemical oxidation. We note that the reduction peak C3, observed even in anhydrous DMSO 0.1 M KCl ultrasonicated solution in the absence of any organic compound, was related to the activity of the Pt electrode [24] and will be not discussed here. The potential values  $E_p$  corresponding to peaks A1, C1 and C2, issued from the voltammetric response, are listed in Table 5.

Since the A1 anodic potentials values were indicative of the electron donating strength of the compounds, we considered that these potentials also reflect their oxidation easiness, i.e. increasing with the decrease of the oxidation potential value.

Our attention was primarily focused on the pair of peaks A1/C1. Thus, by comparing voltammograms of the bis(*p*-aminophenol)-based diamino-chloro-*s*-triazine **1b** with its *O,O'*-diacetyl analogue **2** (Fig. 2A), the disappearance of peak A1, around 0.020 V versus Ag/AgCl,  $KCl_{sat}$ , proved that this was due to absence of the free *p*-HO-phenolic group in **1b**, involved in the first step of oxidation. That is, the replacement of *p*-HO (from **1b**) by the *p*-AcO group (in **2**) leads to peak A1 vanishing, i.e. the single NH group in **2** was unable to trigger any oxidation process. We note that, in the case of *paracetamol*, containing just one *p*-aminophenol unit, a recent well-documented *N*-acetyl-*p*-benzoquinonimine oxidation product is mentioned in the literature as a result of a reversible A1/C1 two-electron transfer process (Scheme 4) [25a–c].

The above redox pathway occurs in spite of the low  $\epsilon_{HOMO}$  level (Table 2) and low LPN(H) orbital population of *paracetamol* (Table 3). As shown in Table 5, under our conditions, the peak A1 of *paracetamol* was located at a negative value,  $-0.027$  V versus Ag/AgCl,  $KCl_{sat}$ .

Therefore, concerning the oxidation stage, we postulated a similarity between the EW influence of the variable  $\pi$ -deficient *s*-triazine ring linked to the NH group in our compounds and that of the EW Ac group in *paracetamol*. If so, as for *paracetamol*, the pair of peaks A1/C1 also disclosed an overall and reversible two-electron transfer process/*p*-aminophenol unit even for compounds **1b** and **3a** exhibiting positive  $E_p$  A1 values (Table 5). Thus, in a two-step oxidation process, a novel extended  $\pi$ - $\pi$ -conjugated system of type (*s*-triazinyl)-*p*-benzoquinonimine was formed (Scheme 5).

One should observe that the decreasing order of the A1 peak potentials (Table 5), for example in the (G-O) dendron

<sup>2</sup> According to the definition from Ref. [22b]: “Fixed in a single conformation either by geometric constraints or because of an overwhelmingly on-sided conformational equilibrium.”

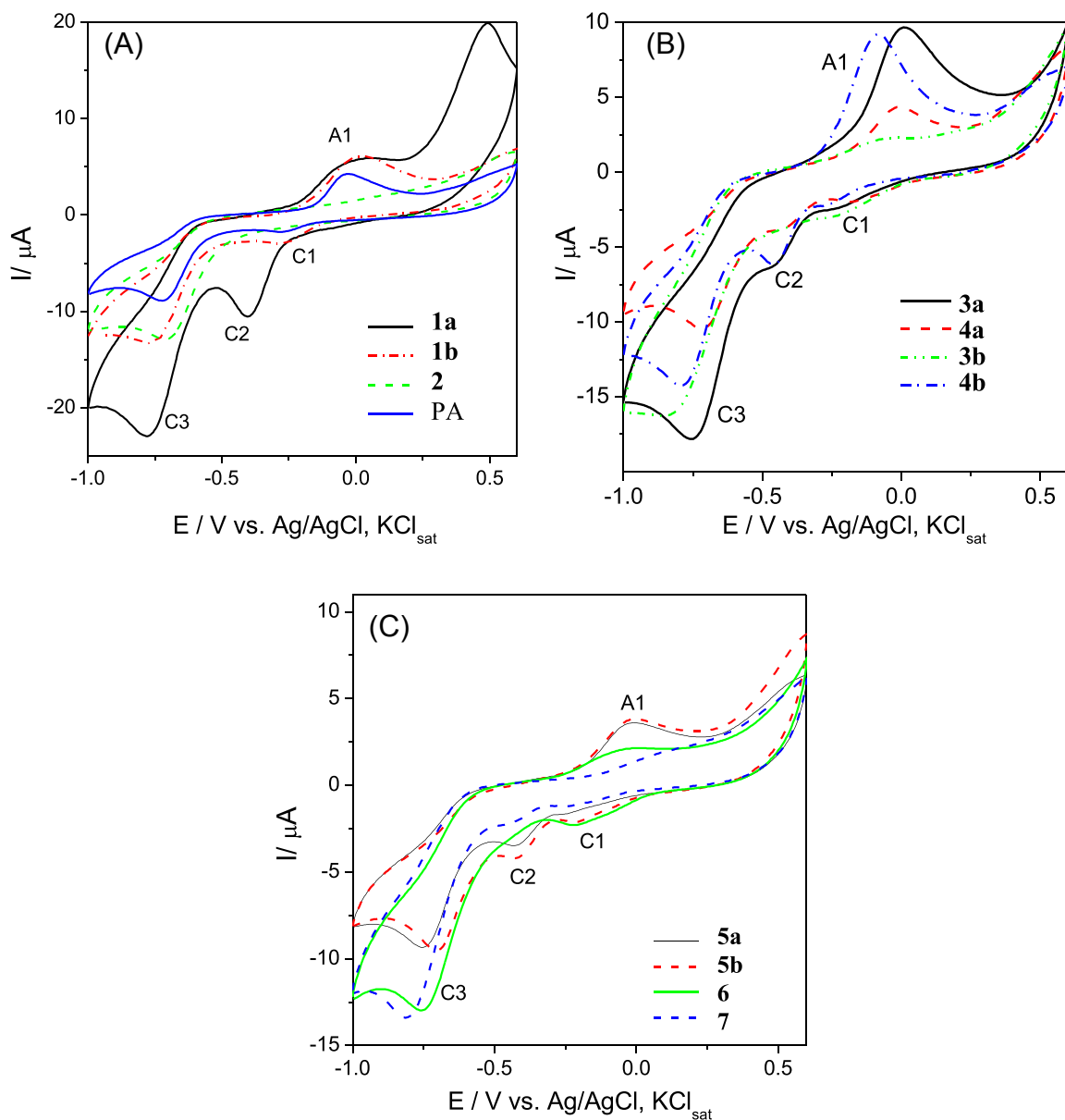


**Fig. 2.** Cyclic voltammograms of  $10^{-3}$  M *paracetamol* (PA), **1a**, **1b**, **2** (2A), **3a**, **3b**, **4a**, **4b** (2B) and **5a**, **5b**, **6**, **7** (2C). Experimental conditions: electrolyte, anhydrous and ultrasonicated DMSO/0.1 M  $\text{KCl}_{\text{sat}}$  solution deaerated with Ar; starting potential  $-1$  V versus Ag/AgCl,  $\text{KCl}_{\text{sat}}$ ; scan rate,  $0.050 \text{ V}^{-1}$ ; the 25th cycle is shown.

series as **1b** > **1a** > **3a** > **3b**, was parallel to the decreasing strength of the  $\pi$ -deficiency of the EWG *s*-triazine expressed as  $\epsilon_{\text{HOMO}}$  values (Table 2) or LPN(H) orbital populations (Table 3). They crucially determined the

adjacent NH group ability for oxidation. Therefore, we assumed the *p*-benzoquinonimine route (Scheme 5) to be valid for all derivatives exhibiting the pair of peaks A1/C1 (Fig. 2) and the unique electronic transfer for compounds

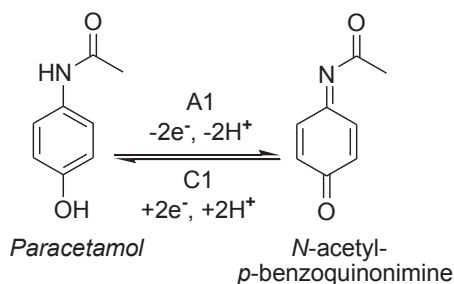
**Table 5**

Values of A1, C1, C2 peaks potential of compounds *paracetamol* (PA), **1a**, **1b**, **2**, **3a**–**5a**, **3b**–**5b**, **6** and **7** (for Experimental conditions, see Fig. 2).

Compound $E_p$ (V) vs. Ag/AgCl, $\text{KCl}_{\text{sat}}$											
	<b>1b</b>	<b>1a</b>	<b>3a</b>	<b>4a</b>	<b>5a</b>	<b>5b</b>	PA	<b>6</b>	<b>3b</b>	<b>4b</b>	<b>2</b>
A1	0.020	0.015	0.013	−0.015	−0.021	−0.024	−0.027	−0.048	−0.052	−0.090	— <sup>a</sup>
C1	−0.270	—	−0.230	−0.180	−0.245	−0.210	−0.275	−0.205	−0.220	−0.275	−0.240
C2	—	−0.400	−0.440	−0.415	−0.430	−0.420	—	—	—	−0.460	−0.440

<sup>a</sup> Too weak to be measured.





Scheme 4.

**1b**, **3b** and **6** (Table 5). Nevertheless, to what amount this route involved, simultaneously, all *p*-aminophenol peripheral units could not be established because of the iterative nature of the oxidation process.

Furthermore, the influence of several other factors concerning the redox process A1/C1 (Scheme 5) was also observed. Thus, (G-0) dimeric melamines **4a** and **4b** disclosed significantly lower anodic oxidation potentials against (G-0) monomeric melamines **3a** and **3b**, respectively, most probably because of a better NH-solvation in DMSO expressed by TG values (Table 4).

A comparison between the CVs of (G-0) melamines **3a** and **3b** (Fig. 2B) showed that the replacement of the piperazine-1-yl ligand with the more electron-donor 4,4-bipiperidin-1-yl dramatically decreased the anodic oxidation potential, i.e. from +0.013 V to -0.052 V versus Ag/AgCl, KCl<sub>sat</sub>. We associated this behaviour with the higher basicity of **3b** versus **3a** together with the different conformational nature of their diaza-linkers, flipping in **3a** but anancomeric in **3b** (Scheme 3). Consequently, the adsorption on the electrode surface of **3b** was more intimate in comparison with that of **3a**. Presumably for the same conformational reason, a similar fluctuation was observed in the case of dimeric (G-0) melamines **4a** (-0.015 V) and **4b** (-0.090 V). *Mutatis-mutandis*, the CVs of the (G-0) melamine **3a** against its dimer **4a** from one hand or of **3b** against **4b** on the other hand (Fig. 2B) exhibited a comparable enhancement of the oxidation current in the case of dimers due, very likely, to the doubling of the number of peripheral phenolic groups and to the symmetry of the molecule.

Similar concepts applied in the case of angularly built (G-1) dendrons **5a**, **5b** and **6**.

The oxidation potential values corresponding to peak A1 in these compounds revealed that **5a**, **5b** and **6** (Fig. 2C) behave similarly in what the easiness of the oxidation was concerned. However, the oxidation current intensity was much smaller in the case of (G-1) melamine **6** with respect to its (G-1) chlorodendron precursor **5a**, presumably because of the blocking of the electrode surface by adsorption of the compound **6** oxidation products.

It is important to notice that, for compound **7** (Fig. 2C), the oxidation peak A1 almost disappeared, suggesting that the dendrimer was much more difficult to oxidize than all its precursors. This behaviour could be motivated by the vaulted spatial arrangement (Fig. 1) of **7**, which impeded the contact between the redox centres of the dendrimer and the Pt electrode surface.

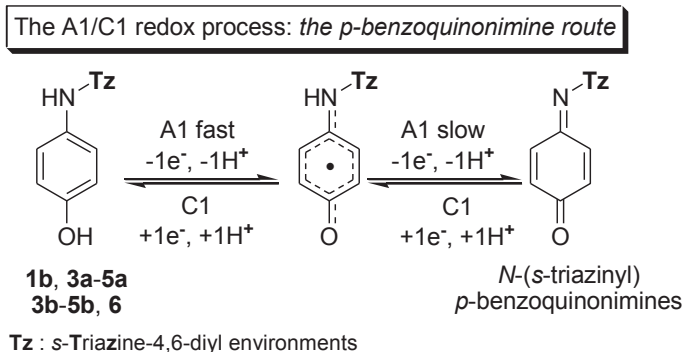
### 2.3.2. Influence of the starting potential

In order to investigate the influence of the starting potential on the electrochemical response of compounds, dimeric G-0 dendron **4a** was selected as a typical example (Fig. 3).

As expected, the width of the scanned potential domain was proven to be of great importance. Starting from an enough negative value of potential (e.g., at least -0.7 V versus Ag/AgCl, KCl<sub>sat</sub>), the appearance of the oxidation peak A1 and of the subsequent reduction processes responsible for reduction peaks C1 and C2 was noticed. When we limited the potential range to a narrow domain (e.g., -0.525 V to +0.300 V versus Ag/AgCl, KCl<sub>sat</sub>), no characteristic oxido-reduction peaks appeared. Generally, the starting potential for the electrochemical measurements was -1 V versus Ag/AgCl, KCl<sub>sat</sub>. If the experiment was done within a large potential window (-1.0 V to +0.6 V), reversing the scan direction (e.g., starting from +0.6 V versus Ag/AgCl, KCl<sub>sat</sub>), no influence on the shape of the voltammogram was observed (Fig. 3).

### 2.3.3. Reproducibility

The reproducibility of the voltammetric measurements was investigated by recording 3 successive voltammograms for the same electrode with cleaning of its surface between measurements. The reproducibility of cyclic



Scheme 5.

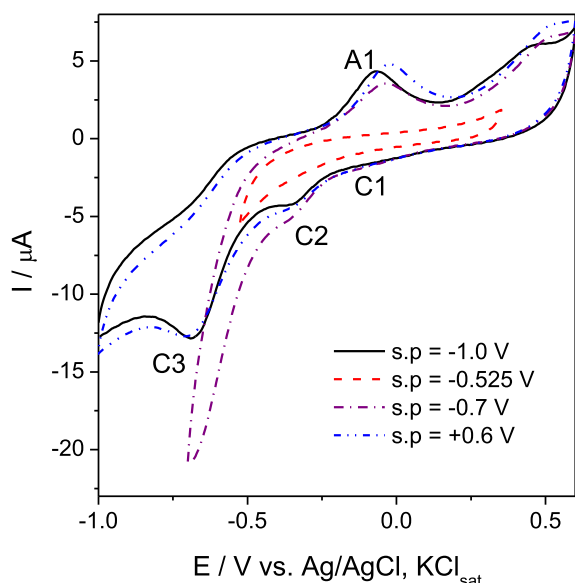


**Fig. 3.** Cyclic voltammogram of  $10^{-3}$  M **4a** at different values of starting potential. Experimental conditions: electrolyte, anhydrous and ultra-sonicated DMSO/0.1 M  $\text{KCl}_{\text{sat}}$  solution deaerated with Ar; scan rate,  $0.050 \text{ V s}^{-1}$ ; the 7th cycle is shown.

voltammetric measurements for compound **4a** was good. Thus, for a mean value of the peak current intensity of  $9.48 \times 10^{-6} \text{ A}$ , for 3 successive measurements the relative standard deviation (RSD) was 11.9% (results not shown).

#### 2.3.4. Influence of repetitive potential cycling

Dimeric (G-0) melamine dendrons **4a** and **4b**, having a low *s*-triazine  $\pi$ -deficiency, were selected in order to study the influence of repetitive potential cycling on the electrochemical response under potentiodynamic conditions by continuous cycling of the electrode potential (25 cycles) in the potential range of  $-1 \text{ V}$  to  $+0.6 \text{ V}$  versus Ag/AgCl,  $\text{KCl}_{\text{sat}}$ , in DMSO solution, on the Pt electrode. The results are shown in Fig. 4.

A progressive increase of the peak current was observed suggesting a possible polymerization taking place on the Pt electrode surface. We note that the electropolymerization of *p*-aminophenol on the Pt electrode in organic media leading to a soluble and electroactive polymer was reported by Taj et al. [9a] as early as 1992. As proposed in Scheme 6, in our case, the electrochemical pathway should be (i) similar to that of *p*-aminophenol [9h], irrespective of the presence of the *s*-triazinyl fragment and (ii) related to that of *paracetamol* [25d].

Thus, the electrochemical significance of peak A1 was almost the same as that in Scheme 5, fast *p*-HO phenolic against slow NH oxidation, the last one being the most sensitive to the EWG *s*-triazine vicinity. As a result, a radical *o,o'*-coupling, similar to that previously reported for *paracetamol* [25d], occurred to produce dimeric and then linear tetrameric species, respectively, with a *s-trans* arrangement of the *s*-triazine bulky motifs. One must observe that the cathodic peak potential C2 (Table 5) was located at much more negative values in comparison with C1, in agreement with the decreasing order of stability against reduction of

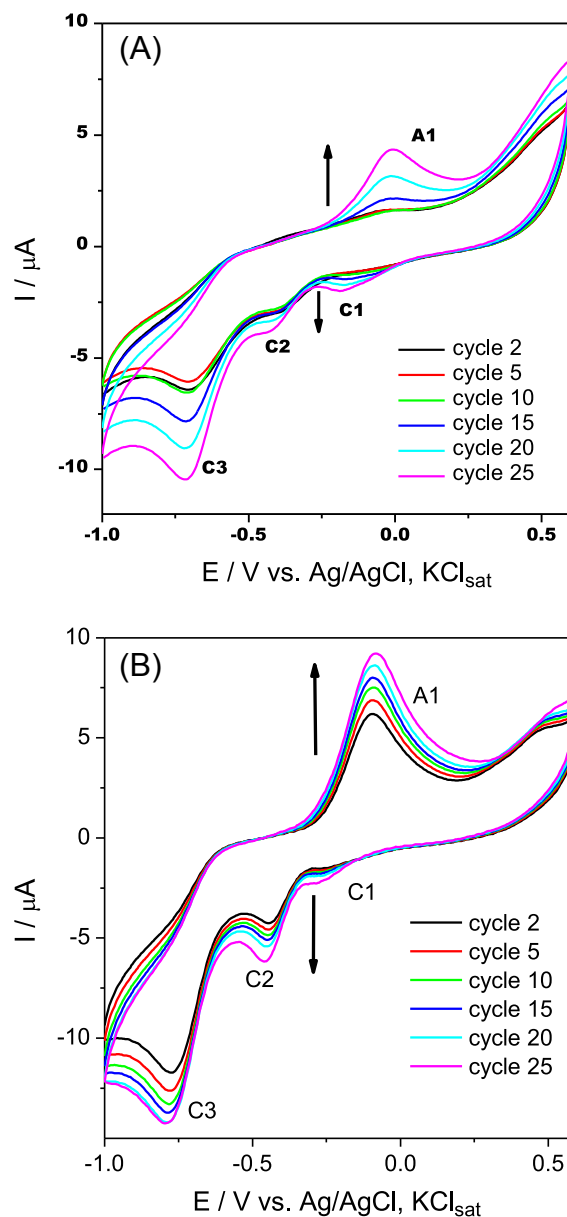
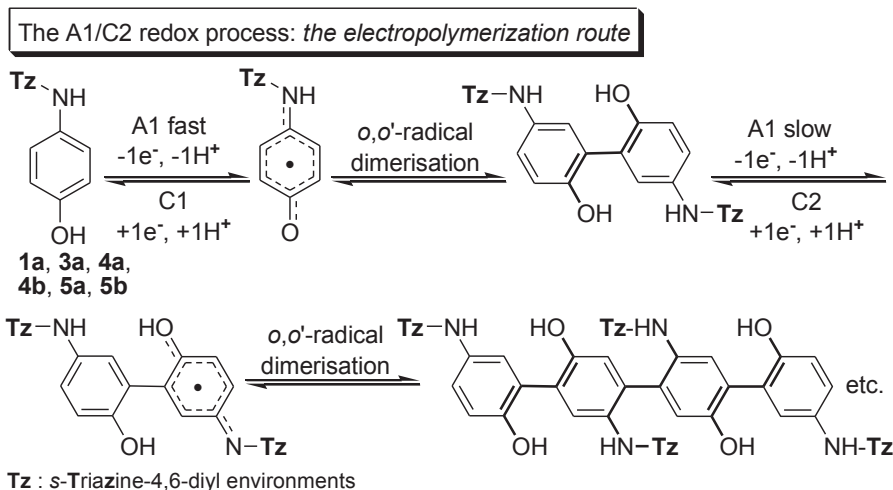


**Fig. 4.** Cyclic voltammograms of  $10^{-3}$  M **4a** (A) and **4b** (B) on the Pt electrode. Experimental conditions: electrolyte, anhydrous and ultra-sonicated DMSO/0.1 M  $\text{KCl}_{\text{sat}}$  solution deaerated with Ar; starting potential,  $-1 \text{ V}$  versus Ag/AgCl,  $\text{KCl}_{\text{sat}}$ ; scan rate,  $0.050 \text{ V s}^{-1}$ .

the involved  $\pi$ - $\pi$ -conjugated system, aromatic (C2) > *p*-benzoquinonimine (C1).

Besides **4a** and **4b**, the electropolymerization route could be extrapolated to all melamines exhibiting the reduction peak C2 namely (G-0) **1a** and **3a**, (G-1) **5a** and **5b**. The electropolymerization route appeared to be the single one in the case of (G-0) melamine **1a** (Fig. 2A); however it was not observed for melamines (G-0) **3b** (Fig. 2B) and (G-1) **6** (Fig. 2C).

In order to perform a quantitative evaluation of the polymer matrix permeability, cyclic voltammograms of compounds **4a** and **4b** were recorded for different potential scan



Scheme 6.

rates on the Pt/**4a** electrode, immersed in a 5 mM  $K_3[Fe(CN)_6]$  solution, containing 0.1 M KCl (results not shown).

The voltammetric wave corresponding to the anodic and cathodic peak currents of the  $[Fe(CN)_6]^{3-}/[Fe(CN)_6]^{4-}$  couple obeys Equation (1):

$$I_p = (2.69 \times 10^5) n^{2/3} A D^{1/2} v^{1/2} C_0 \quad (1)$$

where  $n$  is the number of electrons,  $A$  is the active surface area ( $cm^2$ ),  $D$  is the diffusion coefficient ( $cm^2/s$ ),  $v$  is the scan rate and  $C_0$  is the concentration in bulk solution ( $mol/cm^3$ ).

Using Equation (1), the  $K_3[Fe(CN)_6]$  diffusion coefficient at the Pt electrode was found to be equal to  $3.3 \times 10^{-6} cm^2/s$  which is in concordance with those reported in the literature [26]. Assuming this value for the  $K_3[Fe(CN)_6]$  diffusion coefficient, the area of the modified electrode Pt/**4a** was estimated to be  $0.2226 cm^2$ , which is greater with a factor of 1.13 than the geometrical surface of the electrode ( $0.19625 cm^2$ ), confirming that during the 25 cycling process an immobilization of compound **4a** on the Pt surface occurred.

In addition, the relative increase of the charge transfer on the electrode surface can be estimated by the Equation (2):

$$Q = (Q_{25}/Q_2 - 1) \times 100 \quad (2)$$

where  $Q_{25}$  is the electric charge calculated from the under surface area of the oxidation peak after 25 cycles and  $Q_2$  is the same parameter for the second cycle. In the case of Pt/**4a** and Pt/**4b**, the value of  $Q$  was about 6.54% and 12%, respectively, after 25 continuous cycles, indicating that an activation of the surface took place.

### 3. Conclusions

#### 3.1. Synthesis

Avoiding any protective–deprotective step, the iterative synthesis of a new 10 member family of (G-0, -1, -2)

dendritic melamines comprising *p*-aminophenol (peripheral unit) and piperazine or 4,4'-bipiperidine (linkers) was reported. The chemoselective amination of cyanuric chloride performed with the above amino-nucleophiles was more accessible if piperazine was the internal linker of choice. Overall, the low solubility of these amino-*s*-triazines in common volatile organic solvents and their high relative retention on column chromatography were the two main obstacles to be overcome, successfully, with good yields.

#### 3.2. Structure

DFT calculations in DMSO (with global energy minima, indicative bond order indexes, bond lengths and lone pair orbital populations) helpfully established and discriminated the rotational diastereomerism of *p*-aminophenol peripheral units about the partial double bonds C(*s*-triazine)-N(exocyclic) as being of type *asymmetric* or *anti–anti*. The last one was also localised at the periphery of the first *p*-aminophenol-based (G-2) dendritic melamine which adopted a vaulted global shape. Calculation revealed a lower *N*-lone pair orbital population in Ph–NH units in comparison with that of the phenolic oxygen atom. (VT)  $^1H$  NMR spectroscopy disclosed, by means of temperature gradients, our *p*-aminophenol-based amino-*s*-triazines being not only OH but also strongly  $>N \cdots H \cdots O = SMe_2$  solvated molecules. Solvation was higher if the internal linker was anancomeric (4,4'-bipiperidin-1,1'-diyl) against flipping (piperazine-1,4-diyl); however it was less dependent on the molecular dimension ( $d_H$ ).

#### 3.3. Electrochemical characterisation

Almost all the above structural assignments had an impact on electrochemical characterisation of our amino-*s*-triazines by cyclic voltammetry (Pt electrode/DMSO). A two-electron transfer process was observed. Depending on the variable strength of  $\pi$ -deficiency of the *s*-triazine ring acting as the EWG on the adjacent NH group and the modulation ability of the latter to undergo redox processes in tandem

with the phenolic *p*-HO group, two electrochemical pathways, similar to those already reported for *paracetamol* and *p*-aminophenol were proposed, (i) the *p*-benzoquinonimine route and (ii) the electropolymerization route.

## 4. Experimental

### 4.1. General

Melting points were carried out on an ELECTROTHERMAL instrument. NMR spectra were recorded on a Bruker AM 400, 500 or 600 instrument operating at 400, 500 or 600 and 100, 125 or 150 MHz for  $^1\text{H}$  and  $^{13}\text{C}$  nuclei, respectively. All chemical shifts ( $\delta$  values) are given in parts per million (ppm); all homocoupling patterns ( $^nJ_{\text{H,H}}$  values) are given in Hertz. In the NMR descriptions, some specific abbreviations were used: “br s” (broad singlet), “br d” (broad doublet), “dd app. t” (doublet of doublets appearance as a triplet), “ddd app. td” (doublet of doublets of doublets appearance as a triplet of doublets), Pip (Piperazine linker) and Bipip (4,4'-Bipiperidine linker). TLC monitoring was performed by using aluminium sheets with silica gel 60 F254 (Merck) (visualisation in UV at  $\lambda = 254$  nm). Column chromatography was conducted on Silica gel Si 60 (40–63 mm, Merck). IR spectra were recorded on a JASCO FT-IR 6100 Spectrometer. Only relevant absorption maxima are listed, throughout, in  $\text{cm}^{-1}$ : s (strong), m (medium) and w (weak). Microanalyses were performed on a Carlo Erba CHNOS 1160 apparatus. Mass spectra were carried out on a LTQ ORBITRAP XL (Thermo Scientific) instrument which was externally calibrated using the manufacturer's ESI(+) calibration mix. The samples were introduced into the spectrometer by direct infusion.

Synthesis of compounds **1a**, **1b**, **2**, **3a**, **3b**, **4a**, **4b**, **5a**, **5b**, **6** and **7** together with their full analytical and spectral data are given in the SI (Supporting information).

### 4.2. Computational details

The full geometry optimisation of compounds **1a**, **1b**, **2**, **3a**, **3b** and **7** has been carried out at the DFT level of theory considering the M06-2X [13] exchange-correlation functional together with the def2-TZVP basis set (def2-TZV basis set for compound **7**) [14] in the presence of a solvent environment implemented in the Gaussian 09 [15] program package. The solvent effects have been taken into account via the Polarizable Continuum Model (PCM) using the integral equation formalism variant (IEFPCM) [16] considering the DMSO ( $\epsilon = 46.826$ ) as the solvent environment. No negative wave numbers were obtained for all optimization cases, proving that true minima of the potential energy surfaces were found in the optimisations. Next, the charge distribution and the Wiberg's bond-order index analyses (Table 3) were performed considering the natural population analysis (NPA) [17–20] method through the NBO module built in the Gaussian09 package.

### 4.3. Electrochemical investigation. Reagents and methods

The supporting electrolyte for electrochemical measurements was ultrasonicated DMSO (Merck) containing

0.1 M KCl (Reactivul Bucuresti). The reagents were of analytical grade and used as received.

### 4.4. Electrochemical measurements

Cyclic voltammetry was performed on a PC-controlled electrochemical analyser Autolab-PGSTAT 10, EcoChemie, The Netherlands. Electrochemical experiments were carried out using an undivided cell equipped with three-electrodes: a platinum electrode as the working electrode, a platinum wire as the counter electrode and Ag/AgCl,  $\text{KCl}_{\text{sat}}$  as the reference electrode, respectively. The electrolyte solution was deoxygenated by bubbling argon for 15 min before measurements.

## Acknowledgement

The financial support from a Grant provided by the Research Council Romania (Project PN-II-ID-PCE-2011-3-0128) is gratefully acknowledged. A.B. acknowledges the financial support from the Romanian National Authority for Scientific Research and Innovation (ANCSI) through the Core Program 2015.

## Appendix A. Supporting information

Supporting information related to this article can be found at <http://dx.doi.org/10.1016/j.crci.2016.07.002>.

## References

- [1] (a) A. Petri, European Patent 0,208,376 A2, 14 January 1987.  
(b) A. Petri, European Patent 0,208,376 B1/15 September 1993.  
(c) M. Negoro, K. Kawata, US Patent 2005/0,209,453 A1/22 September 2015.  
(d) M. Negoro, K. Kawata, US Patent 7,135,567/14 November 2006.
- [2] (a) S. Shabbir, S. Zulfiqar, Z. Ahmad, M.I. Sarwar, *Tetrahedron* 66 (2010) 1389;  
(b) S.S. Mahapatra, S. Rana, J.W. Cho, *J. Appl. Polym. Sci.* 120 (2011) 474.
- [3] P. de Hoog, P. Gamez, W.L. Driessen, J. Reedijk, *Tetrahedron Lett.* 43 (2002) 6783.
- [4] (a) S.K. Ghosh, A. Saha, B. Hazarika, U.P. Singh, H.R. Bhat, P. Gahtori, *Lett. Drug Des. Discov.* 9 (2012) 329;  
(b) H.R. Bhat, U.P. Singh, P. Gahtori, S.K. Ghosh, K. Gogoi, A. Prakashe, R.K. Singh, *New J. Chem.* 37 (2013) 2654;  
(c) H.R. Bhat, U.P. Singh, P. Gahtori, S.K. Ghosh, K. Gogoi, A. Prakashe, R.K. Singh, *RSC Adv.* 3 (2013) 2942.
- [5] (a) M. Darabantu, M. Pintea, M. Fazekas, P. Lameiras, C. Berghian, I. Delhom, I. Silaghi-Dumitrescu, N. Plé, A. Turck, *Lett. Org. Chem.* 3 (2006) 905;  
(b) F. Popa, P. Lameiras, O. Moldovan, M. Tomoaia-Cotisel, E. Hénon, A. Martinez, C. Sacalis, A. Mocanu, Y. Ramondenc, M. Darabantu, *Tetrahedron* 68 (2012) 8945;  
(c) O. Moldovan, P. Lameiras, I. Nagy, T. Opruta, F. Popa, C. Antheaume, Y. Ramondenc, M. Darabantu, *Tetrahedron* 69 (2013) 2199;  
(d) O. Moldovan, I. Nagy, P. Lameiras, C. Antheaume, C. Sacalis, M. Darabantu, *Tetrahedron: Asymmetry* 26 (2015) 683;  
(e) V. Lates, D. Gligor, M. Darabantu, L.M. Muresan, *J. Appl. Electrochem* 37 (2007) 631.
- [6] (a) W. Zhang, E.E. Simanek, *Org. Lett.* 2 (2000) 843;  
(b) A.E. Enciso, F. Ramirez-Crescencio, M. Zeiser, R. Redón, E.E. Simanek, *Polym. Chem.* 6 (2015) 5219;  
(c) R.S. Sreepremuduru, Z.M. Abid, K.M. Claunch, H.-H. Chen, S.M. McGillivray, E.E. Simanek, *RSC Adv.* 6 (2016) 8806.
- [7] (a) C.S. Cameron, C.B. Gorman, *Adv. Funct. Mater.* 12 (2002) 17;  
(b) A. Juris, *Annu. Rep. Prog. Chem., Sect. C. Phys. Chem.* 99 (2003) 177.
- [8] (a) J. Wang, G. Rivas, J.R. Fernandes, M. Jiang, J.L. Lopez Paz, R. Waymire, T.W. Nielsen, R.C. Getts, *Electroanalysis* 10 (1998) 553;

- (b) C. Amatore, Y. Bouret, E. Maisonhaute, J.L. Goldsmith, H.D. Abruna, *Chem. Phys. Chem.* 2 (2001) 130.
- [9] (a) S. Taj, M.F. Ahmed, S. Sankarapapavinasam, *J. Electroanal. Chem.* 338 (1992) 347;  
(b) H.J. Salavagione, J. Arias, P. Garces, E. Morallcurron, C. Barbero, J.L. Vazquez, *J. Electroanal. Chem.* 565 (2004) 375;  
(c) Y. Song, *Spectrochim. Acta Part A* 67 (2007) 611;  
(d) H. Yina, Q. Ma, Y. Zhou, S. Aia, L. Zhub, *Electrochimica Acta* 55 (2010) 7102;  
(e) T.A. Enache, A.M. Oliveira-Brett, *J. Electroanal. Chem.* 655 (2011) 9;  
(f) B.N. Chandrashekar, B.E.K. Swamy, M. Pandurangachar, T.V. Sathisha, B.S. Sherigara, *Anal. Bioanal. Electrochem* 3 (2011) 227;  
(g) Ç.C. Koçak, Z. Dursun, *J. Electroanal. Chem.* 694 (2013) 94;  
(h) J. Wang, B. Jin, L. Cheng, *Electrochim. Acta* 91 (2013) 152;  
(i) H. Beiginejad, A. Amani, D. Nematollahi, S. Khazalpour, *Electrochim. Acta* 154 (2015) 235.
- [10] C. Morar, L. Cost, P. Lameiras, C. Antheaume, M. Darabantu, *Synth. Commun.* 45 (2015) 1688.
- [11] (a) T. Drakenberg, S. Forsen, *Chem. Commun.* (1971) 1404;  
(b) S.S. Mirvish, P. Gannett, D.M. Babcock, D. Williamson, S.C. Chen, D.D. Weisenburger, *J. Agric. Food Chem.* 39 (1991) 1205.
- [12] (a) I. Willner, J. Rosengaus, Y.J. Eichen, *Phys. Org. Chem.* 6 (1993) 29;  
(b) A.R. Katritzky, I. Ghiviriga, D.C. Oniciu, A. Barkock, *J. Chem. Soc., Perkin Trans. 2* (1995) 785;  
(c) A.R. Katritzky, I. Ghiviriga, P.G. Steel, D.C. Oniciu, *J. Chem. Soc., Perkin Trans. 2* (1996) 443;  
(d) P. Amm, N. Platzer, J. Guilhem, J.P. Bouchet, J.P. Volland, *Magn. Reson. Chem.* 36 (1998) 587;  
(e) H.E. Birkett, R.K. Harris, P. Hodgkinson, K. Carr, M.H. Charlton, J.C. Cherryman, A.M. Chippendale, R.P. Glover, *Magn. Reson. Chem.* 38 (2000) 504;  
(f) M. Amm, N. Platzer, J.-P. Bouchet, J.-P. Volland, *Magn. Reson. Chem.* 39 (2001) 77;  
(g) I. Ghiviriga, D.C. Oniciu, *Chem. Commun.* (2002) 2718;  
(h) H.E. Birkett, J.C. Cherryman, A.M. Chippendale, J.O.S. Evans, R.K. Harris, M. James, I.J. King, G. Mc Pherson, *Magn. Reson. Chem.* 41 (2003) 324.
- [13] Y. Zhao, D.G. Truhlar, *Theor. Chem. Acc.* 120 (2008) 215.
- [14] F. Weigend, R. Ahlrichs, *Phys. Chem. Chem. Phys.* 7 (2005) 3297.
- [15] Gaussian 09, Revision D.01 M.J. Frisch, G.W. Trucks, H.B. Schlegel, G.E. Scuseria, M.A. Robb, J.R. Cheeseman, G. Scalmani, V. Barone, B. Mennucci, G.A. Petersson, H. Nakatsuji, M. Caricato, X. Li, H.P. Hratchian, A.F. Izmaylov, J. Bloino, G. Zheng, J.L. Sonnenberg, M. Hada, M. Ehara, K. Toyota, R. Fukuda, J. Hasegawa, M. Ishida, T. Nakajima, Y. Honda, O. Kitao, H. Nakai, T. Vreven, J.A. Montgomery Jr., J.E. Peralta, F. Ogliaro, M. Bearpark, J.J. Heyd, E. Brothers, K.N. Kudin, V.N. Staroverov, R. Kobayashi, J. Norm, K. Raghavachari, A. Rendell, J.C. Burant, S.S. Iyengar, J. Tomasi, M. Cossi, N. Rega, J.M. Millam, M. Klene, J.E. Knox, J.B. Cross, V. Bakken, C. Adamo, J. Jaramillo, R. Gomperts, R.E. Stratmann, O. Yazyev, A.J. Austin, R. Cammi, C. Pomelli, J.W. Ochterski, R.L. Martin, K. Morokuma, V.G. Zakrzewski, G.A. Voth, P. Salvador, J.J. Dannenberg, S. Dapprich, A.D. Daniels, Ö. Farkas, J.B. Foresman, J.V. Ortiz, J. Cioslowski, D.J. Fox, Gaussian, Inc., Wallingford, CT USA, 2009.
- [16] J. Tomasi, B. Mennucci, R. Cammi, *Chem. Rev.* 105 (2005) 2999.
- [17] J.P. Foster, F. Weinhold, *J. Am. Chem. Soc.* 102 (1980) 7211.
- [18] A.E. Reed, R.B. Weinstock, F. Weinhold, *J. Chem. Phys.* 83 (1985) 735.
- [19] K.A. Wiberg, *Tetrahedron* 24 (1968) 1083.
- [20] GaussView, Version 5.0.9 R. Dennington, T. Keith, J. Millam, Semi-chem Inc., Shawnee Mission, KS, 2009.
- [21] (a) F. Vögtle, G. Richard, N. Werner, *Dendrimer Chemistry (Concepts, Syntheses, Properties, Applications)*, Wiley-VCH Verlag GmbH & Co. KGaA, 2009, pp. 7–22, 25–44;  
(b) X.K. Moreno, E.E. Simanek, *Macromolecules* 41 (2008) 4108.
- [22] (a) F. Friebolin, *Basic One- and Two-dimensional NMR Spectroscopy*, VCH Verlagsgesellschaft, Weinheim, New York, 1991, pp. 93–263–291;  
(b) E.L. Eliel, H.S. Wilen, *Stereochemistry of the Organic Compounds*, John Wiley & Sons, New York, 1994, pp. 642–1191.
- [23] H. Kessler, *Angew. Chem., Int. Ed. Engl.* 21 (1982) 512.
- [24] V. Tanasković, I. Pašti, S. Mentus, *Int. J. Electrochem. Sci.* 8 (2013) 6243.
- [25] (a) M. Zidan, T.W. Tee, A.H. Abdullah, Z. Zainal, G.J. Kheng, *Int. J. Electrochem. Sci.* 6 (2011) 279;  
(b) A. Asghari, M. Ameri, A.A. Ziarati, S. Radmanna, A. Amoozadeh, B. Barfi, L. Boutorabi, *Chin. Chem. Lett.* 26 (2015) 681;  
(c) C. Engin, S. Yilmaz, G. Saglikoglu, S. Yagmur, M. Sadikoglu, *Int. J. Electrochem. Sci.* 10 (2015) 1916;  
(d) V. Fischer, P.R. West, L.S. Harman, R.P. Mason *Environ. Health Persp.* 64 (1985) 127–137.
- [26] O. Miyawaki, L.B. Wingard, *Biotechnol Bioeng* 31 (1988) 179.